

Air Blast Reflection Ratios and Angle of Incidence

Len Schwer¹

¹Schwer Engineering & Consulting Services

1 Abstract

The Unified Facilities Criteria 3-340-02 provides blast wave reflection ratios as a function of angle-of-incidence in Figure 2-193. However no text is provided indicating the source of this information. A knowledgeable source provided that the figure combines experimental and analytic results. In an effort to assess the UFC information, comparisons are made with two different sets of small scale experiments and LS-DYNA Eulerian simulation results. These comparisons agree fairly well with UFC except in the region of the critical angle-of-incidence, i.e. transition from a regular reflection to a Mach reflection, where there are large differences.

Of interest to LS-DYNA users, the comparisons presented also include the simple expression for reflection ratios as a function of angle-of-incident proposed by Randers-Pehrson and Banister, and used in the LS-DYNA algorithm Load Blast Enhanced. It is shown that the Randers-Pehrson and Banister representation of reflection ratios is a lower bound on the above mentioned Unified Facilities Criteria, experiments and LS-DYNA simulations.

2 Introduction

The Unified Facilities Criteria (UFC 3-340-02) provides Figure 2-193 "Reflected pressure coefficient versus angle of incidence," reproduced here as Figure 1. There is no accompanying text indicating how this chart was developed. In a private email exchange with Dr. Charles Needham (2016), he provided:

"These particular curves were generated from data and theory for square waves on planar ramps."

Note: since only the incident and reflected maxima of the wave forms are required for the reflection ratio, the subsequent shape of the wave form does not matter. Also, these reflection ratios are independent of the source of the wave form, e.g. spherical free air or hemi-spherical surface bursts.

Kingery and Coulter (1983) provide their Figure 9, identical to UFC 3-340-03 Figure 2-193, and reference it as the work of Brode (1970). This report by Brode does not appear to be available via internet searching; it may be classified.

Verification of UFC Figure 2-193 is of interest as it is represented by a simple analytical form, Equation (1), introduced by Randers-Pehrson and Banister (1997) in their LS-DYNA (DYNA3D) implementation of the ConWep air blast algorithms, which in turn are based on the work of Kingery and Bulmash (1984).

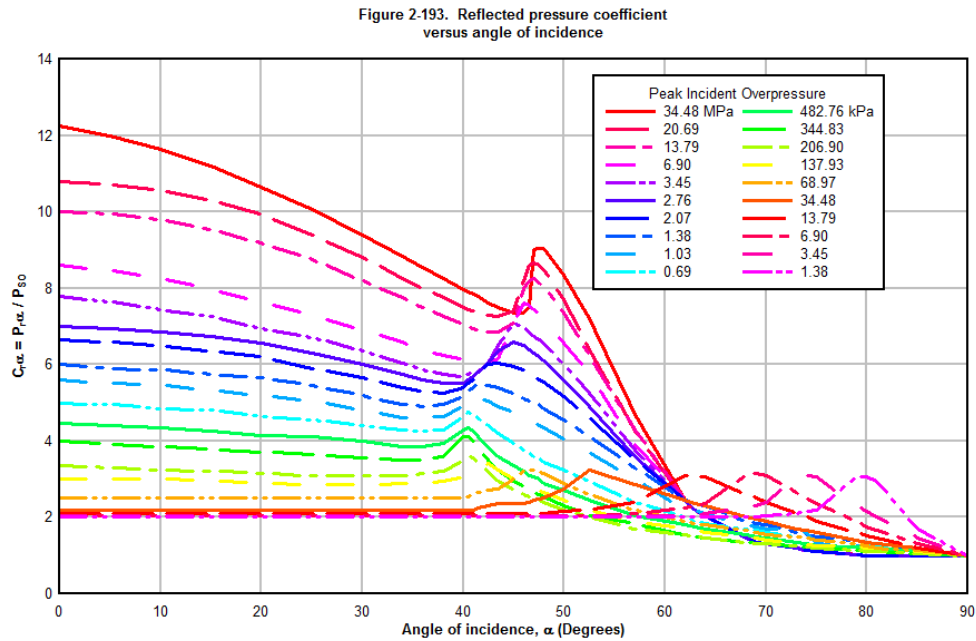


Figure 1 Refection ratio versus angle of incidence (Reproduced from UFC 3-340-02 Figure 2-193).

$$P(t) = P_I (1 + \cos \theta - 2 \cos^2 \theta) + P_R \cos^2 \theta$$

(1)

$$P(t) = P_I \text{ Incident when } \cos \theta = 0 \quad \theta = 90^\circ$$

$$P(t) = P_R \text{ Reflected when } \cos \theta = 1 \quad \theta = 0^\circ$$

For a given incident and reflected pressure, Equation (1) is illustrated in Figure 2. Here the selected incident pressure is $P_I = 34.5 \text{ kPa}$ consistent with one set of values in UFC Figure 2-193, and a reflected pressure of $P_R = 78.2 \text{ kPa}$. This value of incident pressure was selected as it is within the range of the measured incident pressures discussed in the subsequent experiment section. The reflected pressure is provided by the same ConWep calculation that provided the selected incident pressure, i.e. a 1.164g TNT hemi-spherical surface burst charge at 6 meters.

A direct comparison with UFC Figure 2-193 can be made by normalizing the Randers-Pehrson and Banister ordinate of Figure 2 by the incident pressure, see Figure 3. Note: ConWep provides a zero angle of incidence reflection ratio of 2.26 compared to the UCF value of 2.2. Also, the Rankine-Hugoniot relations provide a reflection ratio of 2.297 for this incident pressure and a constant $\gamma = 1.4$.

The reflection ratio comparison in Figure 3 clearly indicates the approximation provided by Randers-Pehrson and Banister significantly underestimates the UFC reflection ratio for most of the AOI range. At larger incident pressures, i.e. 3.45MPa see Figure 4, the difference between the two representations of reflection ratios exists over a more limited range of AOI, but the difference is greatest near the critical angle of 45 degrees.

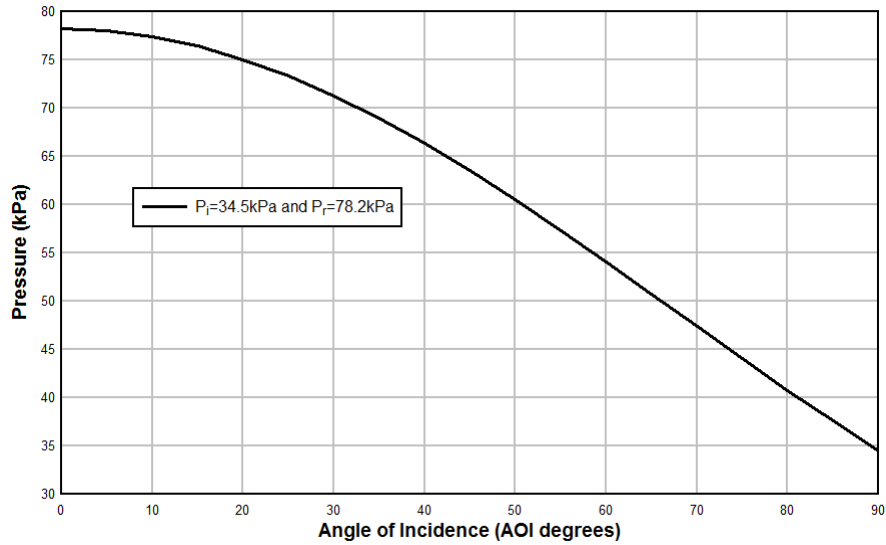


Figure 2 Illustration of Randers-Pehrson and Banister representation of pressure versus AOI.

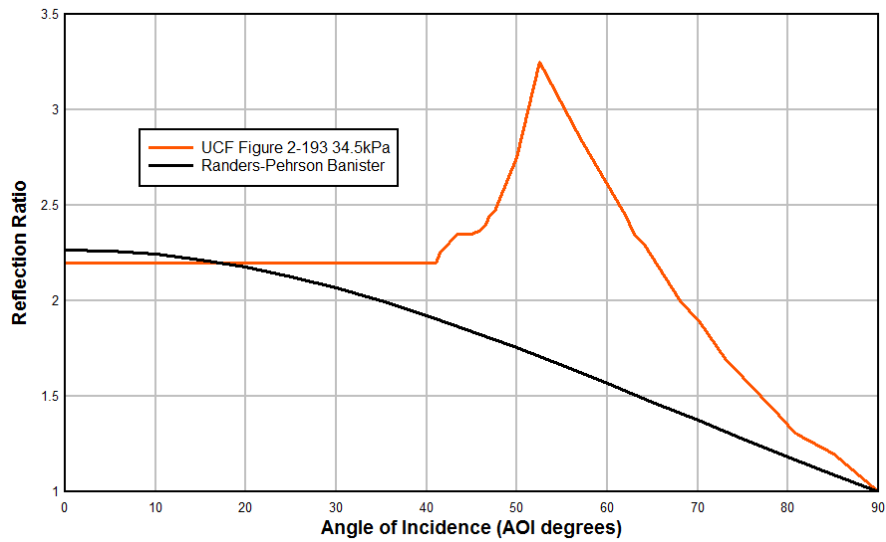


Figure 3 Comparison of reflection ratios from UCF Figure 2-193 and Randers-Pehrson and Banister; for an incident pressure of 34.5kPa.

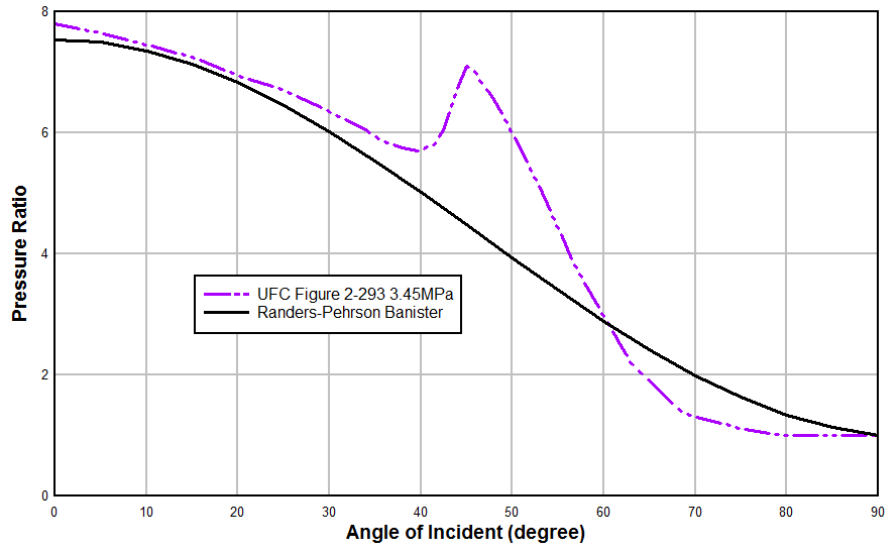


Figure 4 Comparison of reflection ratios from UFC Figure 2-193 and Randers-Pehrson and Banister; for an incident pressure of 3.45MPa.

3 Experimental Assessments of Angle of Incidence

Lacking the detailed explanation in the Brode (1970) report on the source of the UFC Figure 2-193 information, other sources were sought to confirm, or possibly reject, the Figure 2-193 information. Two experimental sources were found: Kingery and Coulter (1983) and Hanus et al (2016). While valuable experimental data, neither group reported repeat experiments or error estimates on their measurement.

3.1 Kingery and Coulter Experiments

Kingery and Coulter used small scale 0.305x 0.305x0.457 meter steel plate targets loaded by detonation of a hemi-spherical surface charge of 1 kg of cast Pentolite (50 PETN, 50 TNT).

“A total of eight peak overpressure levels was (sic) selected and therefore eight models were constructed. Twenty-one angles of incidence were selected with eleven bunched between 37.5 and 62.5 degrees in order to document the transition between regular reflection and Mach reflection.”

The reflection ratio results are presented in their Table 5 and Figure 12 for eight incident pressures; each of the eight incident pressures are given as a pressure pair, e.g. 40.8 and 39.4 kPa, representing the two shots intended to provide the same incident pressure on two different angular orientations of gauges. Figure 5 compares the Kingery-Coulter reflection ratios for the combined incident pressure range 40.8 and 39.4 kPa with the previously presented reflection ratios from UFC 2-193 and normalized Randers-Pehrson & Banister relation. The experimental reflection ratios from Kingery-Coulter generally lie between the UFC Figure 2-193 upper bound and Randers-Pehrson & Banister lower bound. This experimental data suggests a maximum reflection ratio at 50 degrees compared to 52.5 degrees from UFC Figure 2-193.

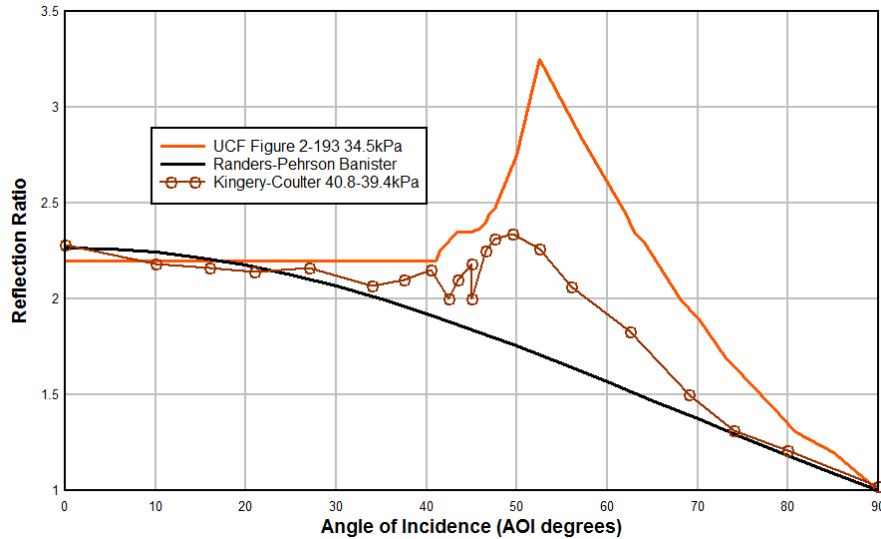


Figure 5 Comparison of reflection ratios from three sources for an incident pressure of about 34.5kPa.

3.2 Hanus et al. Experiments

Hanus et al. (2016) also performed small scale experiments using wooden plates 15 cm wide by 10 cm high by 1.8 cm thick as targets. The blast loading was provided by

“Blast waves are generated from the explosion of a semi-spherical stoichiometric propane/oxygen mixture ($C_3H_8 + 5O_2$) confined in a soap bubble.”

Present Figure 6 shows an illustration of the experimental layout with the targets arranged in a circle of radius 600mm and the soap bubble in the middle. The targets are essentially spaced 10 degrees apart, but the angular position was varied to concentrate some targets in the vicinity of the transition from regular to Mach reflection:

$$\alpha = \frac{381}{\sqrt{P_I + 51}} + 31 \quad (2)$$

here the angle is in degrees and the incident pressure has units of hPa, or millibar.

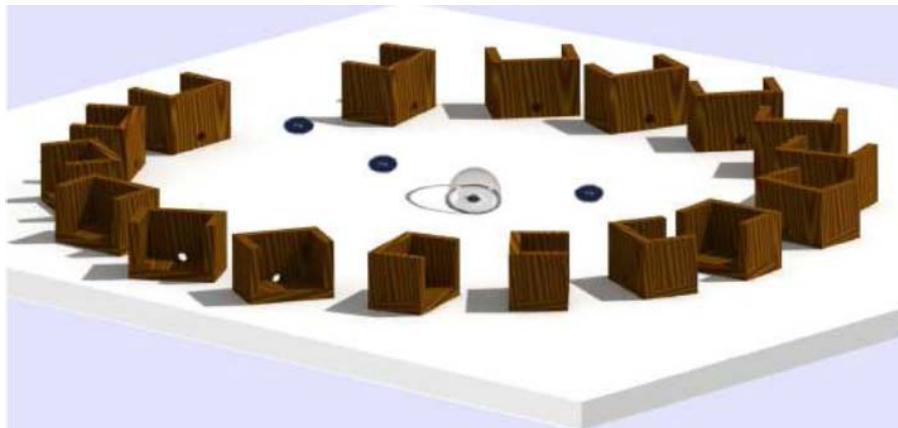


Figure 6 Hanus et al. experimental layout – (Reproduced Figure 4 from Hanus et al.)

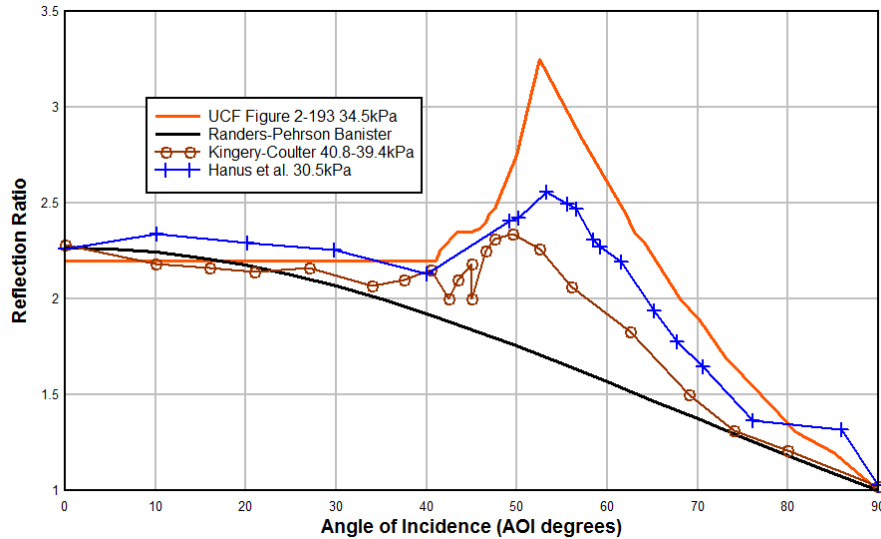


Figure 7 Comparison of reflection ratios from four sources for an incident pressure of about 34.5kPa.

Hanus et al. report results for three incident pressures: 40, 115 and 305 hPa. The largest of these incident pressures, 305hPa, is the closest to the 34.5kPa result from UFC Figure 2-193. Figure 7 compares all the previous reflection ratios with the Hanus et al. data for 30.5kPa. The Hanus data lies between the Kingery-Coulter data and the information from UFC Figure 2-193. The maximum reflection ratio in the Hanus data occurs at 53.2 degrees in close agreement with the UFC maximum angle, and the angle of 51.2 degrees from Equation (2).

4 Numerical Simulation of Angle of Incidence

LS-DYNA calculations were performed in an effort to assess the agreement with the Kingery-Coulter and Hanus et al. data. Several 3D modeling approaches were tried and abandoned as the degree of mesh refinement required to capture the maximum reflected pressure rapidly became excessive. The approach used for the present results combines the LS-DYNA Load Blast Enhanced feature, i.e. ConWep, coupled to an axisymmetric Multi-Material Eulerian solver. Figure 8 shows a typical configuration of the model with the target rotated normal, i.e. 0 degrees, to the radial flow.

The axisymmetric model is a 45 degree radial segment with inner radius of 490mm and outer radius of 800mm. The rigid target has a length of 150mm and is centered at a radius of 600mm, as in the Hanus et al. experiments. The target is embedded in the Eulerian air mesh and coupled to the air via a fluid-structure interface; the LS-DYNA terminology is Constrained Lagrange in Solid. The blast loading is applied to the inner most surface where both the pressure and mass flow act on ambient elements which serve as boundary conditions for the adjacent Eulerian air domain. Three tracer particles monitor the inflow in through the ambient layer (T3) and the free field condition at 600mm (T1 & T2). Five additional tracers are located at the target center aligned with the target normal direction and spaced 1mm apart, starting closest to the target at 599.5mm.

To determine the incident pressure to apply at the inner 490mm boundary that will provide a 34.5kPa incident pressure at the 600mm target range, ConWep was used. First ConWep was run with the requested incident pressure of 34.5kPa and range of 600mm, ConWep provided a TNT charge of 1.164g was required to meet these two constraints. This TNT charge mass was used with LS-DYNA's Load Blast Enhanced keyword and the resulting loading applied to the inner surface of the ambient elements. This boundary condition was verified by running ConWep with the 1.164g TNT charge and comparing the pressure history with the tracer particle located in the ambient layer (T3), see Figure 9.



Figure 8 Illustration of 45 degree axisymmetric sector with target at zero angle of incidence and indicated location of tracer particles.

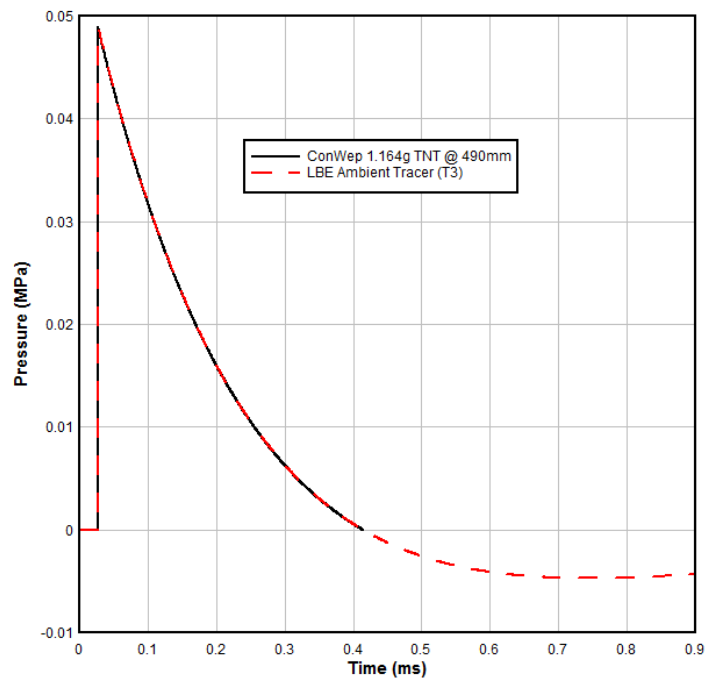


Figure 9 Inner radius boundary condition verification: comparison of ConWep with tracer in ambient layer (T3).

Similarly, the free field pressure at 600mm was verified by comparing the pressure histories at the two LS-DYNA tracers (T1 and T2) with the corresponding ConWep result, see Figure 10. The maximum pressures, for a 0.25mm uniform mesh, at the two tracer locations were identical with a value of 36.4kPa which is 5.5% larger¹ than the ConWep maximum pressure of 34.5kPa.

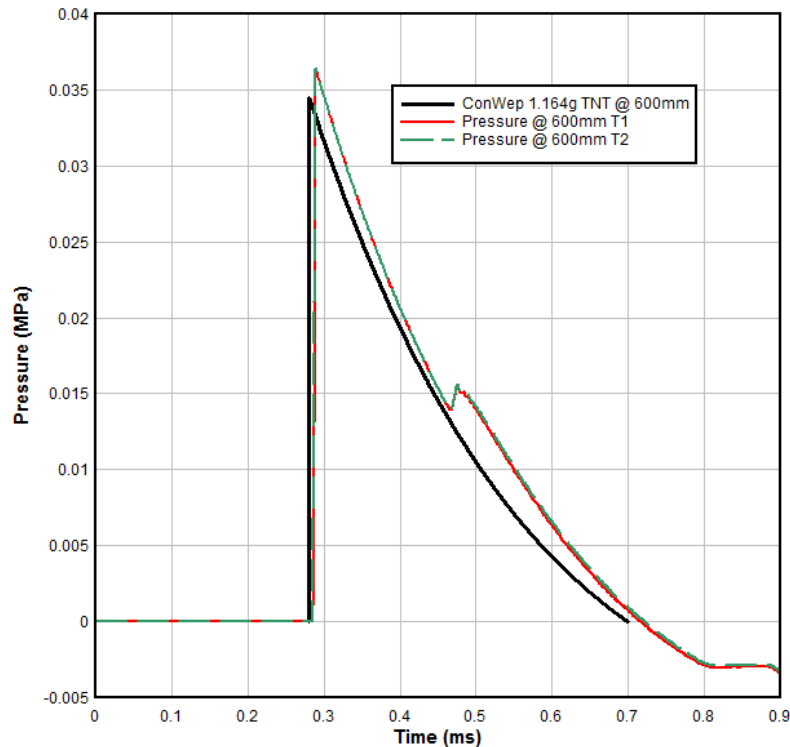


Figure 10 Free field pressure at 600mm verification – comparison of ConWep with tracers T1 & T2.

A mesh refinement study was conducted for four orientations of the target: 0, 45, 52.5 and 90 degrees, see Figure 12. The bar chart shown in Figure 12 provides the results of the mesh refinement study. The 90 degree orientation, i.e. target aligned with the radial flow, was not sensitive to mesh refinement. However, the other three AOI investigated were sensitive to mesh refinement. Both the 0 and 52.5 degree AOI tended to converge² toward values of 2.329 and 2.515, respectively, when Grid Convergence Index (GCI) was applied to the three finest mesh discretizations. The values for the 45 degree angle oscillated rather than converged. The CPU time for the finest mesh, 0.25mm, was about 240 times greater than for the coarsest 2mm mesh.

¹ This numerical overshoot may be due to the mass flow approximation used in conjunction with the prescribed pressure (ConWep) in the ambient layer.

² The three finest mesh results were not in the asymptotic regime required for GCI and hence the GCI did not indicate convergence. As an example consider the zero degree mesh convergence results. The GCI estimated exact numerical result is 2.329. However, the Variable γ Rankine-Hugoniot relations provide a reflection ratio of 2.297 for an incident pressure of 36.4kPa, which is almost identical to the finest mesh result shown in Figure 12. The conclusion is additional mesh refinements are likely necessary to asymptotically approach the value of 2.297

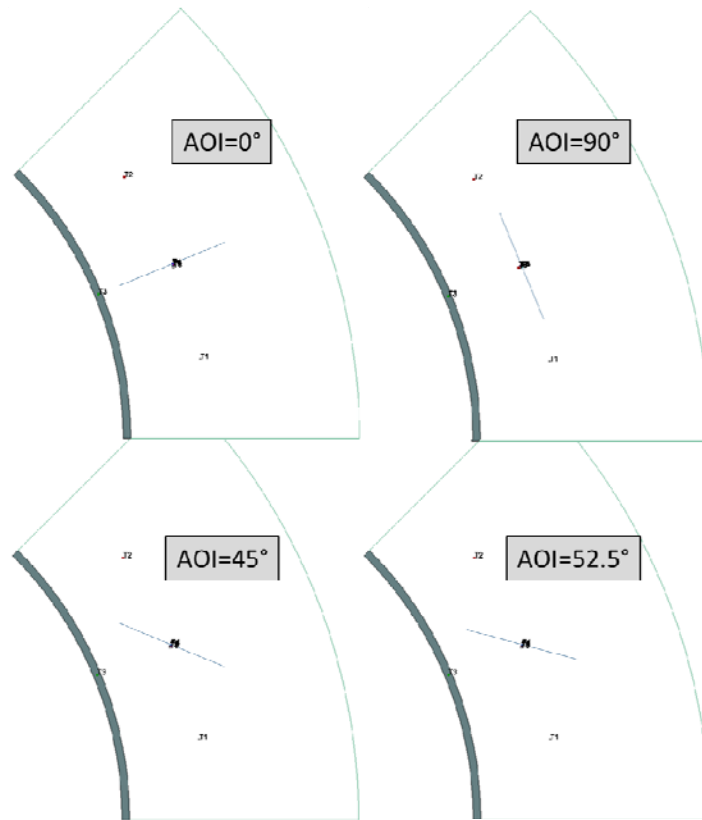


Figure 11 Illustration of target orientations used in mesh refinement study.

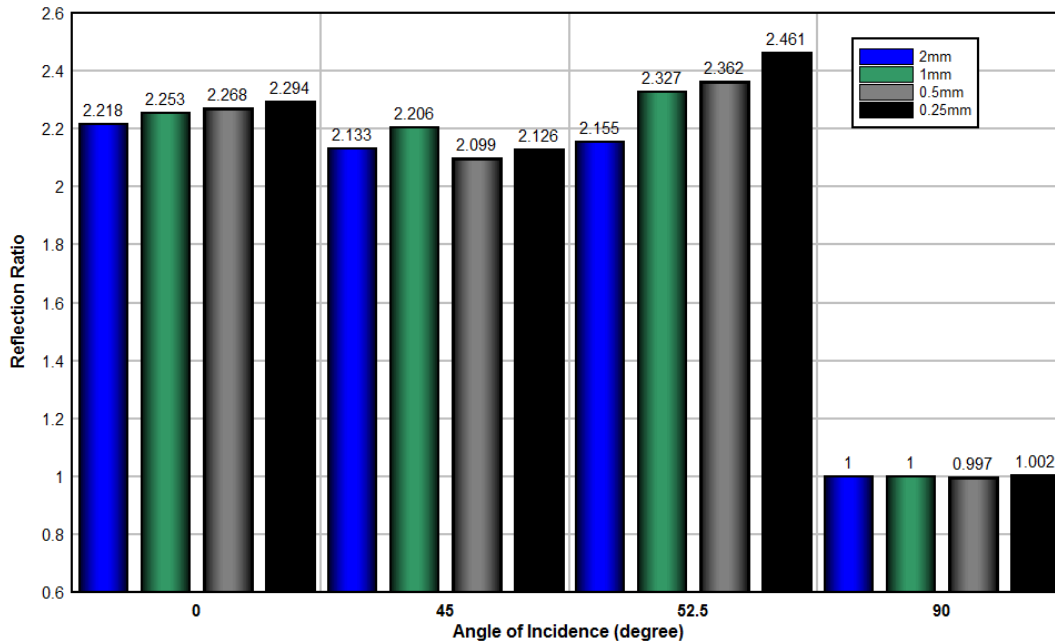


Figure 12 Mesh refinement study from 2 to 0.25mm at four angles of incidence.

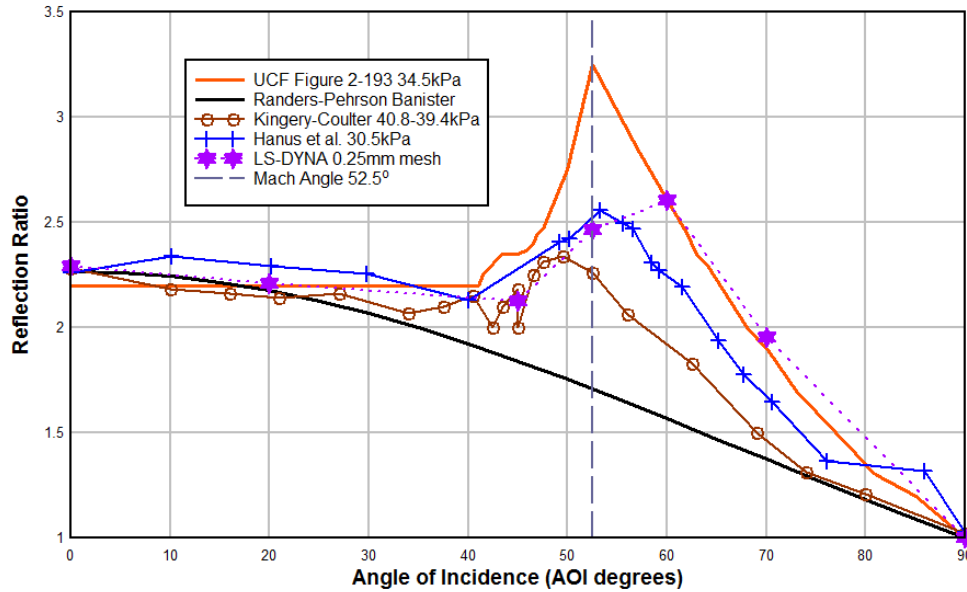


Figure 13 LS-DYNA reflection ratio comparison with the UFC, Randers-Pehrson & Banister and two sets of experimental results.

Figure 13 shows the comparison of the fine mesh (0.25mm) LS-DYNA results with all the previous results. Up to and including the critical angle of 52.5 degrees, the LS-DYNA results agree fairly well with the two sets of experimental results. Interestingly, for angles greater than the critical angle, the LS-DYNA results align with those from UFC Figure 2-193.

Using the UFC Figure 2-193 as a basis, the relative error for the Randers-Pehrson & Banister, two experimental results, and LS-DYNA simulations are provided in Figure 14. For all of the angles examined, the simple analytical representation proposed by Randers-Pehrson & Banister has the largest relative error. The Kingery-Coulter data has more error than the data from Hanus et al. The LS-DYNA results have comparable, or less, error than the two sets of experimental data.

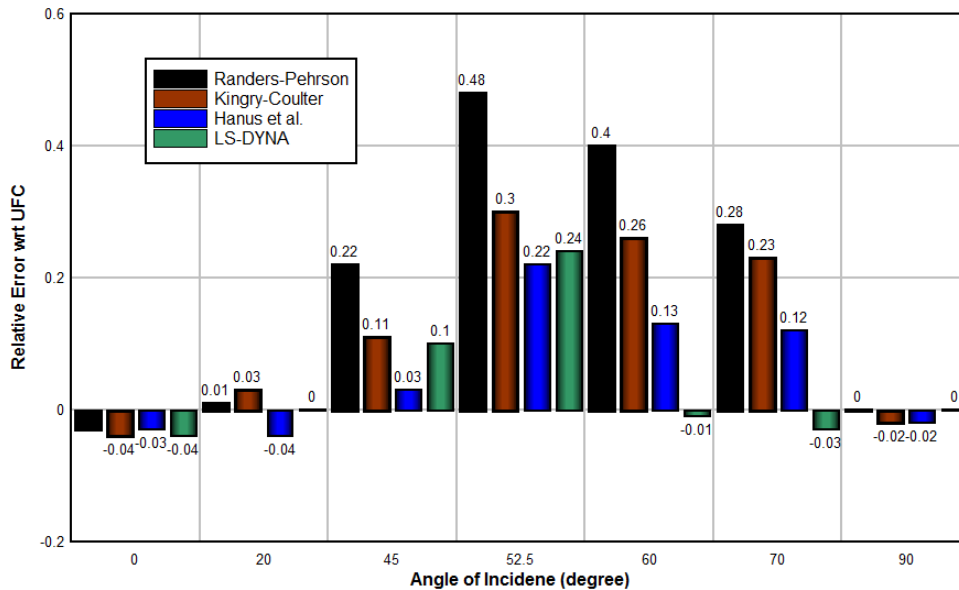


Figure 14 Relative error in reflection ratios with respect to the UFC Figure 2-193 results.

5 Conclusions

Perhaps two important conclusions can be drawn from this study:

1. The simple analytical representation of reflection ratios proposed by Randers-Pehrson and Banister significantly underestimates the ratios in the vicinity of the transition from regular to Mach reflection (critical angle), both with respect to UFC and the two sets of experimental results. Users of the LS-DYNA Load Blast Enhanced feature need to be aware of this limitation.
2. The largest reflection ratios provided by UFC Figure 2-193 could not be substantiated by experiments (two sets) or LS-DYNA simulation results in the vicinity of the critical angle.

Two observations:

1. The maximum pressure ratios from Kingery-Coulter and LS-DYNA do not appear at same angle as UFC Figure 2-193, but the Hanus et al. data agrees with the UFC angle.
2. It would benefit this comparative analysis to know precisely the source of the information in Figure 2-193, i.e. the Brode (1970) reference.

6 Acknowledgement

The author is grateful to Dr. Charles Needham for discussions about the source of the UFC Figure 2-193 reflection ratios. The author is most grateful to Professor Jean-Luc Hanus for discussions related to his reflection ratio experiments and significant suggested improvements in the text.

7 References

UNIFIED FACILITIES CRITERIA (UFC 3-340-02), "Structures to Resist the Effects of Accidental Explosions," 5 December 2008.

Needham, Charles (2016), private email exchange.

Kingery, C. and G. Coulter, (1983) "Reflected overpressure and impulse on a finite structure," ARBRL-TR-02537, Aberdeen, Maryland.

Brode, N.L. (1970) "Height of Burst Effects at High Overpressures," The Rand Corporation, R4-6301, DASA 2506, July 1970.

Randers-Pehrson, G. and K. Bannister, (1997) "AirBlast Loading Model for DYNA2D and DYNA3D," Army Research Laboratory, ARL-TR-1310, March 1997. [Available from www.ntis.gov]

Kingery, C.N. and G. Bulmash, (1984) "Air-Blast Parameters from TNT Spherical Airburst and Hemispherical Surface Burst," ABRL-TR-02555, U.S. Army Ballistic Research Laboratory, Aberdeen Proving Ground, MD, April 1984.

Hanus, J.L., L. Bouazaoui, V. Kreiked (2016) "Blast Wave Reflection: Small-Scale Experiments," 24th International Symposium on Military Aspects of Blast and Shock (MABS). September 18 - 23, 2016, Halifax, Nova Scotia, Canada.